Global Theory of Microtearing Modes in the Tokamak Pedestal

J. L. Larakers,* M. Curie, D. R. Hatch, R. D. Hazeltine, and S. M. Mahajan
Institute for Fusion Studies, University of Texas, Austin, Texas 78712, USA

(Received 2 February 2021; revised 20 April 2021; accepted 7 May 2021; published 4 June 2021)

The pedestal of H-mode tokamaks displays strong magnetic fluctuations correlated with the evolution of the electron temperature. The microtearing mode (MTM), a temperature-gradient-driven instability that alters magnetic topology, is compatible with these observations. Here we extend the conventional theory of the MTM to include the global variation of the temperature and density profiles. The offset between the rational surface and the location of the pressure gradient maximum (μ) emerges as a crucial parameter for MTM stability. The extended theory matches observations on the Joint European Torus tokamak.

DOI: 10.1103/PhysRevLett.126.225001

Introduction.—The high confinement (H-mode) operating regime of tokamaks offers a promising avenue for an effective fusion reactor. The essential characteristic of H-mode is the presence of a narrow region at the edge of the plasma where heat and particle transport is greatly diminished. This region is known as the pedestal. Because of its insulating properties, the pedestal is characterized by steep gradients in temperature and density.

A steep and stable pedestal is highly desirable. The pedestal's large gradients levitate the core plasma temperature and density profiles, improving the temperature and density for fusion reactions. Understanding the mechanisms that abate or even disrupt the pedestal is a prominent goal in the fusion community. The pedestal is also highly dynamic. Its evolution is quasiperiodic with a period of gradient steepening followed by a sudden crash of the gradients. These crashes are experimentally termed edge localized modes (ELMs).

During the gradient steepening cycle, the pedestal hosts a spectrum of saturated fluctuations. Figure 1 displays a typical magnetic spectrogram throughout the ELM cycle from the Joint European Torus with carbon wall (JET-C) tokamak. During the inter-ELM period, the spectrogram displays discrete frequency bands of definite toroidal mode number (n). The frequency bands are a common feature of H-mode pedestals [1–6].

These bands have frequencies close to the diamagnetic frequency [$\omega_{*n} = k_\perp \rho_i v_i \ln(n)'/2$] and collision frequency [$\nu = \sqrt{2}\pi n e^4 \ln(\Lambda)/m_e^{1/2} T^{3/2}$]: $\omega \sim \omega_{*n} \sim \nu$. Here T is the plasma temperature, n the density, $v_i = \sqrt{2T/m_i}$, $\rho_i = v_i/\Omega_i$ the ion gyroradius, $k_\perp = m/r$, m the poloidal mode number, and $\ln(\Lambda)$ the Coulomb logarithm. r is the minor radial coordinate, and the prime represents a radial derivative. The fluctuations occur in the presence of large temperature gradients, correlate with electron heat transport, and have long wavelengths $k_\perp \rho_i < 1$ [6]. All these characteristics match the fingerprint of an instability known as the "microtearing mode" [8].

The microtearing mode [9] (MTM) is an electromagnetic instability that is localized about rational magnetic surfaces and is capable of altering the flux-surface topology. Its growth rate scales with $\omega_{*T} = k_\perp \rho_i v_i \ln(T)'/2$. The real frequency is in the electron direction and is not far from the local diamagnetic frequency: $\omega \approx \omega_{*n} + \omega_{*T}$. It is distinctive from conventional tearing modes [10] by being driven by temperature gradients, with little regard for the conventional stability parameter Δ' [10], and in its dependence on the velocity variation of the Coulomb cross section [9].

The pedestal has many low-order rational surfaces discretely spaced on which microtearing modes could be active. Local gyrokinetic simulations and conventional MTM dispersion relations commonly predict all low-order

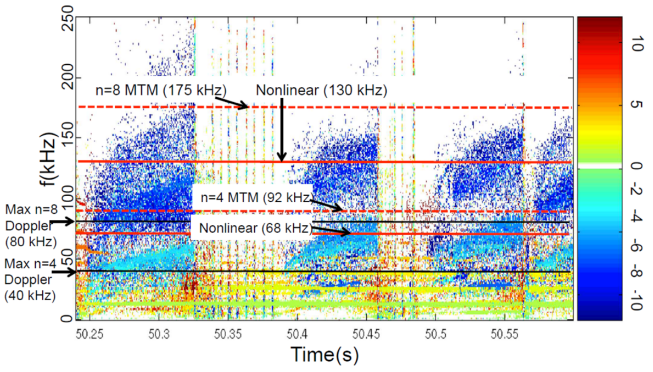

FIG. 1. Magnetic spectrogram showing fluctuations throughout several ELM cycles from JET-C pulse #78697. The vertical broadband lines are ELMs. The inter-ELM bands of fluctuations with toroidal mode numbers $n = -4$ and $n = -8$ are clearly visible. The negative sign indicates the mode is propagating in the electron diamagnetic direction. The low frequency bands with positive n numbers are core modes and not relevant to our study. Figure courtesy of Ref. [7].

rational surfaces as unstable [7,8]. In contrast, global gyrokinetic simulations show that only a subset of rational surfaces have active MTMs [7,8,11]. Microinstabilities are known to be affected by global treatment [12–14]. Motivated by this circumstance and a need for physical understanding, we extend the conventional MTM theory to include global effects.

The key global feature is the strong variation of the drift frequencies ω_{*n} and ω_{*T}, henceforth together referred to as ω_*, in the pedestal. The ω_* variation is nonmonotonic. It is maximal near the mid pedestal, and away from the peak it decays. Despite the many theoretical studies of microtearing [9,15–20] and more recent gyrokinetic simulations [12,21–24], a basic analytical investigation of the impact of global ω_* variation on the MTM is not available.

The aforementioned gyrokinetic studies [7,11] analyzed the unstable rational surfaces and found that they all lie near the peak in ω_*. This observation has demonstrated considerable power in explaining the distinctive fluctuation bands [6]. The rational surfaces that are radially offset from the peak are stable and lead to gaps in frequency and mode number. We term this observation "offset stabilization." In this Letter, we present an analytical and numerical study of the electromagnetic equations to explain offset stabilization. The results match with both gyrokinetic simulations and experimental data. This provides additional evidence that MTMs are the major source of magnetic fluctuations and transport in between ELMs.

There are two physical reasons for offset stabilization: (i) At the peak in ω_{*T}, the driving energy is maximized. (ii) The ω_* profile and magnetic shear profile modulate the spatial structure of the mode. If the rational surface and the peak in ω_* align, these influences cooperate to trap the mode and enhance its growth rate. If the rational surface and the ω_* peak do not align, these influences compete and diminish the mode.

Setup.—Unconstrained motion along field lines allows magnetic surfaces to arrive at local thermal equilibrium on a fast timescale R/v_e. Here, $v_e = \sqrt{2T/m_e}$, and R is the major radius. Slower transport across surfaces sets up radial gradients. Here, by radial we mean the direction across magnetic surfaces. The microtearing mode is an instability about this quasistationary state.

We neglect the curvature of the toroidal geometry. This effectively brings our model into a Cartesian slab. We define x to be the radial direction and the origin $x = 0$ to coincide with a rational surface of interest. The perpendicular directions y and z lie in the planes of the magnetic surfaces. The z direction coincides with the direction of the magnetic field on the rational surface.

The magnetic field direction changes radially. We define $1/L_s = (r/qR)(\ln q)'$, $1/L_n = (\ln n)'$, and $1/L_T = (\ln T)'$ to characterize the magnetic shear and the quasistationary gradients; q is the safety factor. The dimensionless quantities $\hat{s} = L_n/L_s$, $\beta = 8\pi n_e T/B^2$, and $\eta = L_n/L_T$ will also be used.

The microtearing mode arises from the solution to suitably ordered versions of Ampere's law and quasineutrality ($\rho_i/a \ll 1$, $\omega \sim \omega_{*n} \sim \nu$, $\beta \ll 1$, $k_\perp \rho_i \ll 1$). a is the minor radius of the tokamak. These equations describe an electromagnetic perturbation with wave vector $\mathbf{k} = k_\perp \hat{y}$ and frequency ω. They have been repeatedly discussed in the past literature [9,17,18].

$$\frac{d^2 A_\parallel}{dx^2} = -\frac{4\pi}{c}\sigma_\parallel(\omega, x) E_\parallel \tag{1}$$

$$\left(\frac{c}{v_A}\right)^2 \omega(\omega - \omega_{*n}) \frac{d^2\Phi}{dx^2} = -4\pi k_\parallel \sigma_\parallel(\omega, x) E_\parallel \tag{2}$$

Here $E_\parallel = i\omega A_\parallel/c - ik_\parallel \phi$ and $k_\parallel = \hat{b}\cdot\mathbf{k}$. Because of magnetic shear, $k_\parallel$ varies in the radial direction. It can be shown that $k_\parallel = k_\perp x/L_s$. The perturbed densities of quasineutrality [Eq. (2)] and the conductivity $\sigma_\parallel$ have been computed using kinetic theory. With boundary conditions on $A_\parallel$ and Φ, this becomes a generalized eigenvalue problem. The microtearing mode is a single branch of solutions. It has the largest growth rate in the parameter regime of interest.

For our analysis, we normalize all length scales to $\rho_s = \sqrt{2}\rho_i$ and frequencies to a representative value of ω_{*n}. The equations become

$$\epsilon \frac{d^2\psi}{dx^2} = \sigma(\psi - x\phi) \tag{3}$$

$$\epsilon \frac{d^2\phi}{dx^2} = \frac{2x}{\omega(\omega - \omega_{*n})}\delta\sigma(\psi - x\phi), \tag{4}$$

where $\psi = \omega A_\parallel$ and $\phi = \hat{s}c/v_i\Phi$. We can identify $\epsilon = m_e/(m_i\beta)$ and $\delta = \hat{s}^2/\beta$ as small parameters. Here ϵ is a conventional small parameter in fusion plasmas and δ is the inverse of a large parameter, $\hat{\beta}$, known to be important to the MTM [25].

The normalized conductivity σ is computed from the electron drift-kinetic equation [26]. It has the form

$$\sigma(\omega, x) = i([\omega - \omega_{*n}(x) - \omega_{*T}(x)]L_{11} - \omega_{*T}(x)L_{12}) \tag{5}$$

Here, the "transport coefficients" L_{11} and L_{12} are functions of $k_\parallel v_e$, ν, and ω. The $k_\parallel$ dependence arises from the fact that particles respond differently to perturbations along the magnetic field and perpendicular to it. These functions contain the entire spectrum of electron response, from adiabatic ($k_\parallel v_e \gg \omega, \nu$) to resonant ($\omega \sim k_\parallel v_e$) to hydrodynamic ($\omega, \nu \gg k_\parallel v_e$) [26]. Since $k_\parallel$ is spatially varying, all three of these regimes can be sampled by the MTM. These transport coefficients vary with a characteristic

length scale $x_\sigma = \omega L_s/k_\perp v_e$; they are localized about the rational surface, decaying to zero at large $k_\parallel$. Clearly, magnetic shear controls the size of x_σ.

Also clearly, the spatial variation of ω_* will affect σ. We denote the length scale of ω_* variation by x_*. This length scale is intimately tied to the width of the pedestal and of the same order. The effect of the ω_* profile on the mode will increase as the ratio $r = x_\sigma/x_*$ increases. A survey of H-mode pedestals, discussed in the following section, has determined that this ratio ranges from 0.02 to 0.6 in the pedestal. Even for small values of this ratio, including the global spatial dependence is important in determining the stability. The spatial dependence of ω_* typically breaks the even and odd symmetry of the microtearing mode equations.

Reduction.—Above we claimed that the ω_* profile and shear profile act together to determine the spatial structure of the mode. Here, we exploit the small parameters ϵ and δ to support this claim. Our ordering restricts us to modes that have length scales $w \gtrsim \rho_s$, where w is the radial mode width. To balance the smallness of ϵ, it follows that

$$\sigma(\omega) \lesssim \epsilon. \tag{6}$$

Formally, to the zeroth order in ϵ, the dispersion relation becomes $\sigma(\omega) = 0$, a well-known result and the original MTM dispersion relation [8,9].

We proceed to higher order. Using $x \sim x_\sigma$ and $\sigma \sim \epsilon$ as upper limits, we see that the right-hand side of Eq. (4) is $\mathcal{O}(\delta^{1/2}\epsilon^{3/2})$. To first order, $\phi = 0$, and we are left with the equation

$$\frac{d^2\psi}{dx^2} - \frac{1}{\epsilon}\sigma(x,\omega)\psi = 0. \tag{7}$$

This equation is conveniently in the form of a Schrödinger equation in which σ/ϵ acts as a potential.

By plotting the structure of σ, we find that alignment of the ω_* peak and the rational surface lead to cooperation and a deeper, stronger well. An offset weakens the well and dampens the mode.

Numerical solution.—We now proceed to the full numerical solution of Eqs. (1) and (2). Our numerical solution is a 3-point stencil finite difference scheme. The discrete system is set up as a homogeneous linear problem with an unknown eigenvalue in the matrix. The eigenvalue ω appears in a nonlinear way in the equations (through σ). A secant method is applied to compute the eigenvalue [27]. We compute tearing parity eigenfunctions and enforce that the eigenfunctions are zero at a sufficient distance from the rational surface. When there is even or odd symmetry breaking, we identify MTMs by continuity with the symmetric case.

The conductivity model is taken from recent work [26]. It is in the form of a matrix-valued continued fraction, derived from projecting the drift-kinetic equation, including the full collision operator, into Sonine polynomials. Truncation at five Legendre polynomials and seven Laguerre polynomials gives good convergence. Our code has been benchmarked with previous work [16] by using the Lorentz gas conductivity.

To study these equations, a parameter survey was performed. It included ten H-mode pedestals from the DIII-D National Fusion Facility and the JET-C facility. The parameters were computed using an equilibrium reconstruction of the temperature, density, and q profile with the code E-FIT [28,29]. The reconstruction is time-averaged over the ELM cycle. The survey provided these parameter ranges: $\hat{s}$: (0.005,0.05), η: (1.0,3.5), β: (0.0005,0.002), ν/ω_*: (0,10), and x_*/ρ_s: (7.0,20.0).

ω_* variation.—The spatial variation of ω_* in the pedestal is modeled by

$$\omega_{*n}(x) + \omega_{*T}(x) = \omega_{\text{peak}} \exp\left(\frac{-(x-\mu)^2}{x_*^2}\right). \tag{8}$$

Since $x = 0$ is the position of the rational surface, μ represents a displacement of the peak in ω_* from that surface. For simplicity, we assume ω_{*n} and ω_{*T} have the same spatial dependence, a circumstance that is appropriate in the pedestal.

We solve Eqs. (3) and (4) numerically and vary μ and r. To elucidate the necessity of ω_* variation, we compute the growth rate with the full dependence given in Eq. (8) and contrast it to uniform ω_*. The uniform ω_* value is determined by evaluating Eq. (8) at the local position of the rational surface.

Figure 2 contrasts the scans for different r values and the different ω_* treatments. It is clear that the local uniform

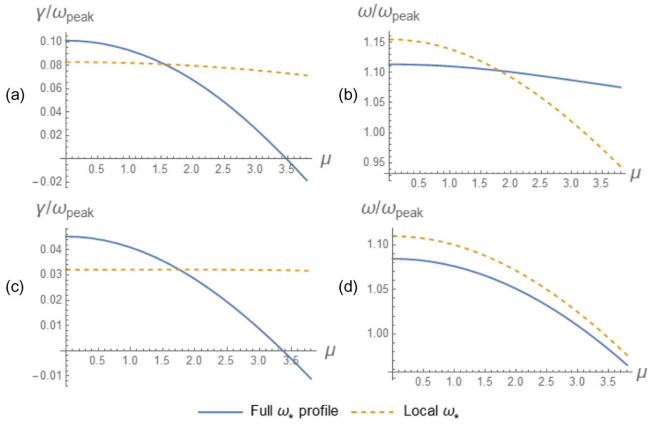

FIG. 2. Growth rate and real frequency of the mode as μ is increased. The blue line indicates the growth rate computed using the full spatial dependence of ω_*. The orange line (dotted) shows the growth rate if ω_* is evaluated at the rational surface and treated as uniform (i.e., the local approximation). (a) and (b) show the eigenvalue corresponding to $r = 0.28$ and $\hat{s} = 0.006$. (c) and (d) correspond to $r = 0.14$ and $\hat{s} = 0.012$. Other parameters are set to $x_*/\rho_s = 10.0$, $\beta = 0.002$, $\nu/\omega_{\text{peak}} = 1.0$, and $\eta = 2.0$.

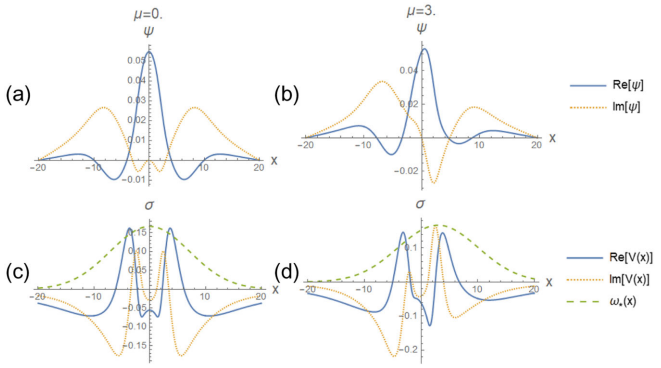

FIG. 3. The eigenmode and the conductivity evaluated at ω. (a) and (c) correspond to the rational surface and ω_* peak aligning, and (b) and (d) correspond to an offset of $\mu = 3.0$. The eigenvalues were determined to be $\omega/\omega_{\text{peak}} = 1.084 + 0.045i$ and $\omega/\omega_{\text{peak}} = 1.009 + 0.009i$, respectively. Parameters were set to $x_*/\rho_s = 10.0$, $\beta = 0.002$, $\hat{s} = 0.012$, $\nu/\omega_{\text{peak}} = 1.0$, $\eta = 2.0$, $Z_{\text{eff}} = 1.0$, and $m_i/m_e = 1836$. Here, $V(x) = i\sigma$.

approximation does not match the more accurate full spatial variation. We observe offset stabilization, that is, the MTM is only unstable when the rational surface is near the peak in ω_*.

Figure 3 displays the eigenfunctions and the conductivity when the peak in ω_* aligns and when it does not. The plots show how ω_* profile influences σ and how the conductivity influences the eigenmode.

Comparison with JET observations.—We conclude by comparing our model to a recently published gyrokinetic study and an experimental spectrogram of JET-C pulse #78697 (shown in Fig. 1) [7]. The gyrokinetic simulations were performed using the code GENE [30,31], including the entire toroidal magnetic geometry. Realistic radial profiles of electron temperature, q, *inter alia*, were computed from experimental diagnostics. The study performed both global linear simulations, considering poloidal mode coupling and profile variation, and local linear simulations. To establish matching of the simulations with the experimental spectrogram, the nominal equilibrium profiles were modified within the error bars. The temperature gradient was increased by 20% and the q profile was reduced by 5%. The local linear simulations computed unstable MTMs at all low-order rational surfaces, while the global simulations selected only the rational surface near the peak in ω_* as unstable.

To perform a comparison of these results to our model, we fit the ω_* profile to a Gaussian and located the positions of rational surfaces with the q profile. Local values of $\hat{s}$, β, ν, and η were extracted for each rational surface; the full variation of these parameters was shown to insignificantly affect the growth rates. Growth rates were computed for each rational surface using uniform and nonuniform ω_*. Under the uniform approximation, all the toroidal mode numbers (up to 12) were found to be unstable.

Global linear GENE [7] and our global reduced model both indicate that only the rational surface $q = 2.75$ associated with $n = 4, 8, 12$ is unstable. Figure 4 provides a full comparison. The $n = 4$ and $n = 8$ modes are observed in the magnetic spectrogram. The real frequencies from linear simulations slightly overestimate the frequency of the fluctuations. Nonlinear simulations performed in [7] provide corrections to capture the proper frequency. The $n = 12$ mode does not appear in the magnetic spectrogram (likely due to the more rapid decay of magnetic fluctuations at smaller scales [7]). Beyond these considerations, the observation that solely $n = 4$ and $n = 8$ fluctuations appear provides evidence that these discrete fluctuation bands arise from micro-tearing modes.

Because of the large experimental uncertainty in the q profile (up to 20% relative error [32]), the locations of the rational surfaces are not known to great precision (approximately $10\rho_s$). Consequently, the framework described here should not be interpreted as having the capability of predicting frequency bands but rather the ability to reproduce them within experimental uncertainties.

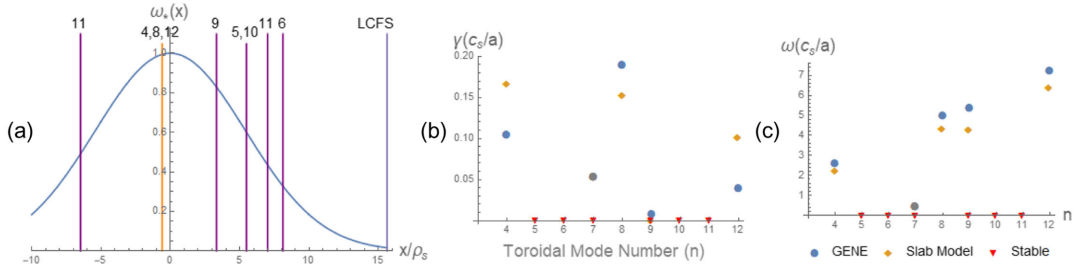

FIG. 4. Here, we display the comparison of the slab model to global linear gyrokinetic electromagnetic numerical experiment (GENE). (a) Displays the Gaussian fit of the ω_* profile and the location of the rational surfaces determined from the q profile. (b) Displays the growth rates of each toroidal mode number. (c) Displays the real frequencies of the unstable modes. The stable markers indicate a negative growth rate for both the slab model and GENE (excluding $n = 7$ and $n = 9$). $n = 7$ (gray) is predicted to be unstable by GENE; however, due to the large jump in real frequency *inter alia*, it is not an MTM. $n = 9$ is predicted to be unstable by GENE, but the growth rate is marginal.

Conclusion.—In this Letter, we have extended the conventional theory of microtearing modes by including the global variation of the ω_* profiles. We have demonstrated that the ω_* profile and the magnetic q profile form the potential well of the mode. The q profile enters by virtue of the spatial dependence of the nonadiabatic electron response $L_{1i}[k_\parallel(x)]$.

This extension has proven to be fruitful. Our model identifies a crucial and until now unknown parameter for the stability of the MTM. It was shown that displacement (μ) of the rational surface from the peak in ω_* quickly stabilizes the mode. We reason this is due to the breakdown of the potential well. This leads to a simple yet powerful condition for MTM instability in the pedestal: the rational surface must lie near the peak in ω_* for it to be unstable.

Armed with this extended model, we produced additional evidence that microtearing modes are a major source of magnetic fluctuations during the inter-ELM cycle. We examined and compared our model to a spectrogram from JET. Our model predicts the same frequency bands and mode numbers as unstable. The unstable mode numbers correspond to rational surfaces that nearly align with the ω_* peak. The uniform ω_* approximation, in contrast, predicts all mode numbers as unstable and a broadband spectrum of magnetic fluctuations. The vast differences in the global and local predictions nullify local treatments for studying MTM stability in the pedestal.

These results provide a simple and expedient framework for determining if microtearing modes are the source of magnetic fluctuations in the pedestal. Future work will focus on applying this framework to larger datasets to solidify this hypothesis. A solid understanding of these fluctuations is a necessary ingredient for modeling the structure and evolution of the pedestal.

We thank Ehab Hassan for his encouragement and for his assistance gathering pedestal parameters. This work was supported by the Department of Physics at the University of Texas at Austin, General Atomics subcontract 4500076923, and by the U.S. Department of Energy ER54742 and ER54698.

*Corresponding author.
j_larakers@utexas.edu

[1] C. P. Perez, H. R. Koslowski, T. C. Hender, P. Smeulders, A. Loarte, P. J. Lomas, G. Saibene, R. Sartori, M. Becoulet, T. Eich, R. J. Hastie, G. T. Huysmans, S. Jachmich, A. Register, and F. C. Schüller, Washboard modes as ELM-related events in JET, Plasma Phys. Controlled Fusion **46**, 61 (2004).

[2] A. Diallo, J. W. Hughes, M. Greenwald, B. Labombard, E. Davis, S. G. Baek, C. Theiler, P. Snyder, J. Canik, J. Walk, T. Golfinopoulos, J. Terry, M. Churchill, A. Hubbard, M. Porkolab, L. Delgado-Aparicio, M. L. Reinke, A. White, and AlcatorC-Modteam, Observation of Edge Instability Limiting the Pedestal Growth in Tokamak Plasmas, Phys. Rev. Lett. **112**, 115001 (2014).

[3] A. Diallo, R. J. Groebner, T. L. Rhodes, D. J. Battaglia, D. R. Smith, T. H. Osborne, J. M. Canik, W. Guttenfelder, and P. B. Snyder, Correlations between quasi-coherent fluctuations and the pedestal evolution during the inter-edge localized modes phase on DIII-D, Phys. Plasmas **22**, 056111 (2015).

[4] M. Cavedon, R. Dux, T. Pütterich, E. Viezzer, E. Wolfrum, M. Dunne, E. Fable, R. Fischer, G. F. Harrer, F. M. Laggner, A. F. Mink, U. Plank, U. Stroth, and M. Willensdorfer ASDEX Upgrade Team, On the ion and electron temperature recovery after the ELM-crash at ASDEX upgrade, Nucl. Mater. Energy **18**, 275 (2019).

[5] F. M. Laggner, A. Diallo, M. Cavedon, and E. Kolemen, Inter-ELM pedestal localized fluctuations in tokamaks: Summary of multi-machine observations, Nucl. Mater. Energy **19**, 479 (2019).

[6] A. Diallo and F. M. Laggner, Review: Turbulence dynamics during the pedestal evolution between edge localized modes in magnetic fusion devices, Plasma Phys. Controlled Fusion **63**, 013001 (2021).

[7] D. R. Hatch, M. Kotschenreuther, S. M. Mahajan, M. J. Pueschel, C. Michoski, G. Merlo, E. Hassan, A. R. Field, L. Frassinetti, C. Giroud, J. Hillesheim, C. F. Maggi, C. P. von Thun, C. M. Roach, S. Saarelma, D. Jarema, and F. Jenko, Microtearing modes as the source of magnetic fluctuations in the jet pedestal, Nucl. Fusion **61**, 036015 (2021).

[8] M. Kotschenreuther, X. Liu, D. R. Hatch, S. Mahajan, L. Zheng, A. Diallo, R. Groebner, J. C. Hillesheim, C. F. Maggi, C. Giroud, F. Koechl, V. Parail, S. Saarelma, E. Solano, and A. Chankin, Gyrokinetic analysis and simulation of pedestals to identify the culprits for energy losses using 'fingerprints', Nucl. Fusion **59**, 096001 (2019).

[9] R. D. Hazeltine, D. Dobrott, and T. S. Wang, Kinetic theory of tearing instability, Phys. Fluids **18**, 1778 (1975).

[10] H. P. Furth, J. Killeen, and M. N. Rosenbluth, Finite-resistivity instabilities of a sheet pinch, Phys. Fluids **6**, 459 (1963).

[11] E. Hassan, D. Hatch, G. Merlo, M. Halfmoon, M. Curie, M. Kotschenreuther, S. Mahajan, R. Groebner, and A. Diallo, Microtearing Signatures in DIII-D Pedestal (unpublished).

[12] D. Dickinson, Effects of profiles on microinstabilities in tokamaks, Ph.D. thesis, University of York, 2012.

[13] G. L. Falchetto, J. Vaclavik, and L. Villard, Global-gyrokinetic study of finite β effects on linear microinstabilities, Phys. Plasmas **10**, 1424 (2003).

[14] P. A. Abdoul, D. Dickinson, C. M. Roach, and H. R. Wilson, Using a local gyrokinetic code to study global ion temperature gradient modes in tokamaks, Plasma Phys. Controlled Fusion **57**, 065004 (2015).

[15] R. R. Dominguez, M. Rosenberg, and C. S. Chang, Nonlinear theory of high-m tearing modes, Phys. Fluids **24**, 472 (1981).

[16] N. T. Gladd, J. F. Drake, C. L. Chang, and C. S. Liu, Electron temperature gradient driven microtearing mode, Phys. Fluids **23**, 1182 (1980).

[17] J. F. Drake and Y. C. Lee, Kinetic theory of tearing instabilities, Phys. Fluids **20**, 1341 (1977).
[18] S. M. Mahajan, R. D. Hazeltine, H. R. Strauss, and D. W. Ross, Unified theory of tearing modes, Phys. Fluids **22**, 2147 (1979).
[19] R. D. Hazeltine and D. W. Ross, Variational theory of drift and tearing eigenmodes in slab geometry, Phys. Fluids **21**, 1140 (1978).
[20] A. Zocco, N. F. Loureiro, D. Dickinson, R. Numata, and C. M. Roach, Kinetic microtearing modes and reconnecting modes in strongly magnetised slab plasmas, Plasma Phys. Controlled Fusion **57**, 065008 (2015).
[21] D. R. Hatch, M. Kotschenreuther, S. Mahajan, P. Valanju, F. Jenko, D. Told, T. Görler, and S. Saarelma, Microtearing turbulence limiting the JET-ILW pedestal, Nucl. Fusion **56**, 104003 (2016).
[22] X. Jian, C. Holland, J. Candy, E. Belli, V. Chan, A. M. Garofalo, and S. Ding, Role of Microtearing Turbulence in DIII-D High Bootstrap Current Fraction Plasmas, Phys. Rev. Lett. **123**, 225002 (2019).
[23] W. Guttenfelder, J. Candy, S. M. Kaye, W. M. Nevins, E. Wang, R. E. Bell, G. W. Hammett, B. P. LeBlanc, D. R. Mikkelsen, and H. Yuh, Electromagnetic Transport from Microtearing Mode Turbulence, Phys. Rev. Lett. **106**, 155004 (2011).
[24] H. Doerk, F. Jenko, M. J. Pueschel, and D. R. Hatch, Gyrokinetic Microtearing Turbulence, Phys. Rev. Lett. **106**, 155003 (2011).
[25] J. F. Drake, T. M. Antonsen, A. B. Hassam, and N. T. Gladd, Stabilization of the tearing mode in high-temperature plasma, Phys. Fluids **26**, 2509 (1983).
[26] J. L. Larakers, R. D. Hazeltine, and S. M. Mahajan, A comprehensive conductivity model for drift and microtearing modes, Phys. Plasmas **27**, 062503 (2020).
[27] M. H. Meylan and L. Gross, A parallel algorithm to find the zeros of a complex analytic function., ANZIAM J. **44**, 236 (2008).
[28] O. Meneghini and L. Lao, Integrated modeling of tokamak experiments with OMFIT, Plasma Fusion Res. **8**, 2403009 (2013).
[29] O. Meneghini *et al.*, Integrated modeling applications for tokamak experiments with OMFIT, Nucl. Fusion **55**, 083008 (2015).
[30] F. Jenko, W. Dorland, M. Kotschenreuther, and B. N. Rogers, Electron temperature gradient driven turbulence, Phys. Plasmas **7**, 1904 (2000).
[31] T. Görler, X. Lapillonne, S. Brunner, T. Dannert, F. Jenko, F. Merz, and D. Told, The global version of the gyrokinetic turbulence code GENE, J. Comput. Phys. **230**, 7053 (2011).
[32] W. Rowan and K. Gentle (private communications).